InAlAs/InGaAs-MSM photodetectors based on optical cavity using metallic mirrors: THz frequency operation, high quantum efficiency and high saturation current

Maximilien Billet, Sara Bretin, Fuanki Bavedila, Vanessa Avramovic, Xavier Wallart, Christophe Coinon, Jean-Francois Lampin, Guillaume Ducournau, Emilien Peytavit

InAlAs/InGaAs-MSM photodetectors based on optical cavity using metallic mirrors: THz frequency operation, high quantum efficiency and high saturation current

Maximilien Billet, Sara Bretin, Fuanki Bavedila, Vanessa Avramovic, Xavier Wallart, Christophe Coinon, Jean-François Lampin, Guillaume Ducournau, and Emilien Peytavit[a)]

Institut d'Electronique de Microélectronique et de Nanotechnologie, UMR CNRS 8520, Université de Lille, Avenue Poincaré, B.P. 60069, 59652 Villeneuve d'Ascq Cedex, France

Abstract

We present a metallic mirror-based resonant cavity-enhanced InAlAs/InGaAs metal-semiconductor-metal (InAlAs/InGaAs-MSM) photodetector driven by a 1550 nm wavelength illumination. The device shows a quantum efficiency higher than 30 %, a cut-off frequency higher than 100 GHz and a saturation current density above 40 kA/cm^2. As a proof of concept, we demonstrate the generation of 0.25 mW of continuous wave output power at a frequency of 100 GHz via the photomixing of an optical beatnote. This result underlines the potential of InAlAs/InGaAs-MSM for sub-THz and THz optoelectronics applications driven by telecom lasers.

Keywords: ultrafast-photoconductors, THz photonics, MSM, optoelectronics

a) Electronic mail: Emilien.peytavit@univ-lille.fr

The most efficient generation of THz waves by photomixing (i.e. optical heterodyne) based on 1550 nm lasers is achieved by using uni-travelling-carrier (UTC) photodiodes as photomixer.[1–3] However, this device is not suitable for detecting THz waves by optoelectronics heterodyne mixing in which the local oscillator is generated by photomixing because of the very weak dependence of the photocurrent on the bias voltage occurring in this device. Indeed, the photocurrent in UTC photodiodes is almost related to the diffusion of the photo-generated carriers out of the p-doped absorption region and their drift in the collection layer thanks to the pn junction built-in electric field. It is thus very slightly influenced by an external electric field. Admittedly, a stronger dependence appears at high optical pump power when the charge carrier density becomes sufficient to screen the internal electric field allowing for optoelectronics heterodyne mixing detection but with conversion loss higher than 30 dB at 100 GHz, not competitive with electronics heterodyne mixers.[4] This is not the case of the ultrafast photoconductors based on low-carrier-lifetime semiconductors, in which the photocurrent depends on the product of the bias voltage and the incident optical power. For example, low-temperature-grown GaAs (LT-GaAs) photoconductors pumped by lasers working at 800 nm, have been widely used in continuous wave (CW) or pulsed THz spectroscopy systems to generate and to detect efficiently THz waves[5–7] as well as in millimeter wave systems such as photonics-assisted analog-to-digital-converter (ADC).[8–10] Last years, researches have been focused on the development of efficient photoconductors working at 1.55 μm based on LT-$In_{0.53}Ga_{0.43}As$ lattice matched grown on InP substrates in order to take advantage of the turn-key, reliable and low-cost 1.55-μm fiber-components.[11–13] However, its narrow band gap (0.75 eV) mandatory to have interband absorption comes with a low dark resistivity and a low breakdown electric field even after incorporation of LT-InAlAs layers to take advantage of their deep trap levels (<200 Ω.cm).[13] For practical applications in time domain spectroscopy (TDS) or CW THz systems, the epitaxial growth and the design of photoconductors based on InGaAs material have to be carefully optimized depending on whether they are intended to work as emitter or detector.[14] An alternative way is the use of a planar interdigitated InAlAs/InGaAs metal-semiconductor-metal (MSM) photodetector, which has been widely studied more than twenty years ago for optical communications.[15–18] Its

photocurrent characteristic is also a function of both the bias voltage and the optical power while it exhibits a low dark current thanks to InAlAs barriers. Such a device can potentially be useful to generate and detect sub-THz and THz waves driven by telecom lasers. It is however limited by the intrinsic trade-off between its 3-dB cutoff frequency (f_{3dB}) and its quantum efficiency (QE)[15]. For example, if a quantum efficiency close to unity has been achieved on InGaAs MSM having an f_{3dB} around 2 GHz,[19] it reaches only 5 % on devices having an f_{3dB} of 70 GHz.[20]

Basically the response time and then the 3-dB-cutoff frequency of a MSM photodetector is limited by its electrical capacitance (RC time constant τ_{RC}) and by the transit time of the holes (τ_h) and the electrons (τ_e) between the contact electrodes. The latter limit the cutoff frequency to the GHz frequency range when the quantum efficiency is close to unity. It can be explained as follow: the transit times of the photo-generated carriers between the contact electrodes are proportional to the ratio of the electrode spacing (s_f) over the carriers velocity. The bias electric field that drifts the electrons (holes) towards the electrodes decreases with the distance (d) from the layer surface because of the planar electrodes configuration. In first approximation, we can consider that the electric field tends to zero when $d = s_f$. Thus, the photocarriers generated at distance larger than the inter-electrode spacing are not accelerated by the bias electric field which results in a very slow contribution to the photocurrent.[17] The only way to suppress this deleterious effect is to keep the layer thickness (t_h) smaller than the electrode spacing. If we neglect the e-h recombination in the semiconductor layer, which means that each photon absorbed results in one e-h pair collected by the contact electrodes, the maximum QE of a photodetector consisting of an absorbing layer of thickness t_h is given by:

$$\mathrm{QE} = (1-R)(1-e^{-\alpha t_h}) \quad (1)$$

where R is the reflexion coefficient at the air/semiconductor interface and α is the absorption coefficient of the light in the absorbing layer. The QE is indeed, in this case, equal to the absorbance of the active layer. It can be shown that s_f should be lower than 200 nm to ensure a transit-time-related cutoff frequency of a MSM-InGaAs photodetector higher than 100 GHz.[18] By using Eq. 1, a

planar MSM InGaAs photodetector of layer thickness t_h = 200 nm (R ≈ 30 % and α ≈ 1 μm^{-1} at λ=1550 nm in $In_{0.53}Ga_{0.47}As$)[21] exhibits a QE of around 10 %. Here, we show that it is possible to obtain simultaneously a high QE (QE > 30 %), a large saturation current density (> 40 kA/cm^2) and a high cutoff frequency (f_{3dB} > 100 GHz) by putting the active layers in an optical cavity in which the contact electrodes also serve as cavity mirrors. We also show that, used as photomixer, this optical cavity MSM photodetector can generate up to 250 μW of output power at a frequency of 100 GHz. The semiconductor structure of our device is sandwiched between two gold mirrors/electrodes forming an optical resonant cavity [see Fig. 1(a)]. The top face mirror consists of a nanostructured semitransparent gold grating[22,23] [see Fig. 1(b)] while the backside mirror is a thick uniform gold layer. The superior properties of the nanostructured semitransparent top mirror in terms of optical losses at 1550 nm and low parasitic serial resistance has been already demonstrated in previous works.[2,24] The semiconductor stack, grown by molecular beam epitaxy, consists of an $In_{0.53}Ga_{0.47}As$ absorption layer of thickness t_{InGaAs} surrounded by two graded $In_{0.52}Al_{0.48}As$ / $In_{0.53}Ga_{0.47}As$ multilayers (total thickness $t_{InAlGaAs}$) followed by two $In_{0.52}Al_{0.48}As$ (thickness t_{InAlAs}) layers [see Fig. 1(c) and Fig. 1(d)]. InAlAs layers are added to raise the Schottky barrier height around 0.7 eV (instead of 0.2 eV on InGaAs) and then to reduce drastically the dark current. InAlAs/InGaAs graded multilayers have been introduced to limit the charges storage at the InAlAs/InGaAs interface by smoothing the conduction band energy level. Here, we set $t_{InAlGaAs}$ = 27 nm and t_{InAlAs} = 30 nm on the basis of the work of Kim and coworkers[25]. Optimization of the optical cavity is performed by using a numerical calculation of the light absorption at normal incidence in the InGaAs layer as a function of its thickness and the geometrical parameters of the grating [see Fig. 1.(b)] based on the rigorous coupled wave analysis.[26,27] By making the same assumption as in the case of the planar electrode, i.e. by neglecting the e-h recombination, and by keeping in mind that the light absorption is almost constant for angles of incidence up to θ_m ≈ 0.5 rad (not shown here), we can consider that the quantum efficiency is directly the calculated light absorption at normal incidence as long as the device is illuminated by a Gaussian beam of spot width larger than $w_m \approx 2\lambda/(\pi\theta_m)$ ≈ 2 μm and smaller than the active area of the device.[28] We show in Fig. 2 typical theoretical QE's for this

structure plotted as a function of the electrode spacing $s_f = t_{InGaAs} + 2\times(t_{InAlGaAs} + t_{InAlAs})$ when the incident optical beam is polarized parallel to the grating vector. The QE calculated from Eq. 1 corresponding to the planar structure is also shown. We also plotted the transit time-related 3-dB-cutoff frequency (f_{tr}) calculated in the simplest model, in which we assume that every photo-carrier in the active layer has a velocity $v_c = 0.5\times10^7$ cm.s^{-1} equal to the theoretical hole saturation velocity in InGaAs[17]. In this model it can be shown that $f_{tr} = 3.5\ v_c / (2\pi\ s_f)$. It is worth to notice that the optical cavity allows a QE superior to 50 % even if the electrode distance s_f is below 200 nm. This means that it is possible to obtain a high photoresponsivity photodetector with a cutoff frequency above 100 GHz unlike the case of planar MSM.

In order to characterize the device properties at high frequencies, we develop a MSM integrated with a coplanar waveguide (CPW). The device fabrication has been achieved by using a gold-to-gold wafer bonding approach of the semiconductor layers and by e-beam lithography coupled to lift-off and dry etching techniques.[22] A SEM view of the fabricated device integrated to the CPW is shown in Fig. 3. The dc photoresponse experiment was conducted by illuminating an InAlAs/InGaAs-MSM photoconductive test structure of 20×20 μm^2 area by a fiber coupled 1550 nm wavelength laser diode by using a lensed optical fiber of mode field diameter (MFD) equal to 3 μm. The dc photocurrents as a function of the bias voltage V_b measured for several optical powers are shown in Fig. 4. The structure presents a dc photoresponse defined as $\Re = I_{ph}/P_{opt}$ of 0.4 A/W for P_{opt} =5 mW, which slightly decreases down to 0.35 A/W for P_{opt} =20 mW. From the photoresponse $\Re$, the quantum efficiency of a photodetector working at a photon energy hν is given by QE=$\Re\times$hν/q where q is the electron charge. Here, it is thus shown that a 200-nm-electrode-spacing device can achieve a QE of 30 %. Furthermore, the clear double dependence with the optical power and the bias voltage of the photocurrent values shows the possibility to use this photodetector as photomixer, heterodyne receiver or sub-sampler. The efficiency of the Schottky barrier is checked by means of dc dark current measurements. In the inset of Fig. 4 is plotted the dark current density J_{dark} as a function of the bias voltage V_b. For V_b=2 V, the dark current density is equal to 40 nA/μm^2, corresponding to a

dark current of 480 nA for a device with an area of around 12 μm^2 (disk of 4-μm-diameter). It must be compared with the dark current of 60 μA obtained at 2 V with an optimized LT-InGaAs photoconductor of same geometry (by using a dark resistivity ρ_{dark} = 200 Ω.cm).

The dynamic photoresponse properties of 4-μm-diameter InAlAs/InGaAs-MSM photodetectors are characterized by means of a photomixing experiment. It consists in measuring the sub-THz or THz waves power generated when the device is dc biased and illuminated by an optical beatnote produced by two continuous lasers spatially superposed and slightly detuned. The wavelength of both lasers are noted λ_1 and λ_2 corresponding to frequencies noted f_1 and f_2. The beat frequency is then equal to $f_b=|f_1 - f_2|$. A schematic overview of the photomixing experimental setup is shown in Fig. 5. The spatial overlapping of the two lasers is achieved with a 50/50 fiber coupler and a first half-wave plate allows for setting the two optical waves in the same polarization state. The beatnote is polarized with an electric field parallel to the grating vector by means of the second half-wave plate.[22] The same lensed fiber as previously is used to illuminate the device under test. The sub-THz power generated in the InAlAs/InGaAs-MSM at the beat frequency is out-coupled in the 50-Ω-CPW, then collected by a 110-GHz coplanar probe and finally sent into a thermal power sensor. A bias-tee is inserted between the probe and the thermal power sensor in order to bias the photodetector. In Fig. 6 is shown the measured output power as a function of the beat frequency generated by a photoconductor of diameter d = 4 μm at a bias voltage V_b= 4 V and an average optical power of P_{opt}=16.8 mW. The losses induced by the coplanar probe, and the Bias-T are measured and are taken into account. It can be noticed that this device presents a cut-off frequency higher than 100 GHz. Furthermore, by increasing the optical power up to P_{opt}=25 mW, we obtain at a frequency of 100 GHz, an output power P_{THz} = 0.25 mW at a bias voltage of 4.4 V and a dc-photocurrent of 5.5 mA. The dc-photoresponse of 0.25 A/W is constant as a function of the optical power at least up to P_{opt} = 25 mW. It means that the small electrode spacing (and then the high surface capacitance) mitigates the electric field screening coming from the charge storage at high optical illumination due to the difference in mobility between the holes and electrons. We obtain here a high saturation current

density of 44 kA/cm^2 . An analytical model of the dynamic photomixer behavior is also developed. If we assume that the MSM acts as a perfect photoconductance $G_0=I_{dc}/V_b$, the photomixer can be modeled as a current source of internal admittance consisting of its photoconductance G_0 shunted by its capacitance C .The power delivered to load of admittance admittance $Y_L=G_L+jB_L$ can be then calculated by using the following expression[29]:

$$P_L = \frac{1}{2}\frac{\left|F(\omega)I_{dc}\right|^2 G_L}{\left|G_L + G_0 + j(\omega C + B_L)\right|^2} \quad (2)$$

Where G_L and B_L denote the conductance and susceptance of the load, I_{dc} is the measured dc photocurrent and is equal to 2.2 mA and $F(\omega)$ is the frequency response of the MSM and can be calculated with the model from ref.[18]:

$$F(\omega) = \left[\frac{1}{j\omega\tau_e}\left(\frac{e^{j\omega\tau_e}-1}{j\omega\tau_e} - 1\right) + \frac{1}{j\omega\tau_h}\left(\frac{e^{j\omega\tau_h}-1}{j\omega\tau_h} - 1\right)\right] \quad (3)$$

With $\omega = 2\pi f_b$ the beating pulsation, $\tau_e = s_f/v_e$ and $\tau_h = s_f/v_h$ the transit times of the electrons and holes at the velocity[17] $v_e = 0.7 \times 10^5$ m/s and $v_h = 0.5 \times 10^5$ m/s between the electrodes separate by a distance s_f= 194 nm. In this simple model, photo-carriers are assumed to drift at their saturation velocity which means, for example, that the bias electric field is not screened by the space charge created by the large difference in mobility between holes and electrons in InGaAs.

In the parallel plate capacitor approximation and by considering that the relative dielectric constant is uniform and equal to that of InGaAs (ε_r=13.9), the capacitance C is evaluated to be around 8 fF for a device of diameter equal to 4 µm. The load in this set-up consists in the 50-Ω-powermeter seen through the coplanar waveguide followed by the coplanar probe and the bias-T and is calculated from vector network analyzer measurements of each separated element. The theoretical value of P_{THz} as a function of the beat frequency is added on the Fig. 6. A relative good agreement with the measurements is observed, even if there is a vertical shift of 2 dB which comes certainly from the nonlinear dc current-tension characteristic. A 3-dB-cutoff frequency above 100 GHz is far beyond the state of the art for InGaAs-MSM photodetectors, which is typically around few tens of GHz.

To conclude, we have presented a design of InAlAs/InGaAs-MSM placed in an optical resonant cavity with an inter-electrode spacing of only 194 nm. We have shown on large area devices a QE > 30 % and a dc-photoresponse higher than 0.4 A/W. Furthermore, we demonstrate that 4-µm-diameter devices have a cut-off frequency above 100 GHz and current saturation above 40 kA/cm^2 mandatory for sub-THz and THz optoelectronics applications driven by telecom lasers. To underline the potential of the device we have also shown the generation of 0.25 mW of CW output power at a frequency of 100 GHz. The next step will be the use of this device as detector of THz waves by optical heterodyne mixing. This device could be thus used as emitter and detector in THz telecom or THz spectroscopy systems

This work is supported by the French Defense Agency DGA (Direction Générale de l'Armement), the RENATECH network (French Network of Major Technology Centers), the Lille University, and the Région Hauts-de-France.

REFERENCES

[1] T. Ishibashi, Y. Muramoto, T. Yoshimatsu, and H. Ito, IEEE J. Sel. Top. Quantum Electron. **20**, 79 (2014).
[2] P. Latzel, F. Pavanello, M. Billet, S. Bretin, A. Beck, M. Vanwolleghem, C. Coinon, X. Wallart, E. Peytavit, G. Ducournau, M. Zaknoune, and J.-F. Lampin, IEEE Trans. Terahertz Sci. Technol. **7**, (2017).
[3] G. Ducournau, P. Szriftgiser, A. Beck, D. Bacquet, F. Pavanello, E. Peytavit, M. Zaknoune, T. Akalin, and J. Lampin, IEEE Trans. Terahertz Sci. Technol. **4**, 328 (2014).
[4] E. Rouvalis, M.J. Fice, C.C. Renaud, and A.J. Seeds, IEEE Trans. Microw. Theory Tech. **60**, 686 (2012).
[5] E. Brown and K. McIntosh, Appl. Phys. Lett. **66**, 285 (1995).
[6] S. Verghese, K.A. Mcintosh, and E.R. Brown, **71**, 2743 (1997).
[7] A. Roggenbuck, H. Schmitz, A. Deninger, I.C. Mayorga, J. Hemberger, R. Güsten, and M. Grüninger, New J. Phys. **12**, 043017 (2010).
[8] C. Tripon-Canseliet, M. Zegaoui, G. Jestin, C. Coinon, P. Berger, G. Baili, A. Descamps-Mandine, I. Maksimovic, D. Decoster, J.M. Hodé, D. Dolfi, and J. Chazelas, Electron. Lett. **52**, 237 (2016).
[9] J.-M. Delord, J.-F. Roux, J.-L. Coutaz, and N. Breuil, IEEE Photonics Technol. Lett. **21**, 1369 (2009).
[10] E. Peytavit, S. Formont, and J.-F. Lampin, Electron. Lett. **49**, 207 (2013).
[11] A. Takazato, M. Kamakura, T. Matsui, J. Kitagawa, and Y. Kadoya, Appl. Phys. Lett. **91**, 011102 (2007).
[12] R.J.B. Dietz, B. Globisch, M. Gerhard, A. Velauthapillai, D. Stanze, H. Roehle, M. Koch, T. Göbel, and M. Schell, Appl. Phys. Lett. **103**, 1 (2013).
[13] B. Sartorius, H. Roehle, H. Künzel, J. Böttcher, M. Schlak, D. Stanze, H. Venghaus, and M. Schell, Opt. Express **16**, 9565 (2008).
[14] B. Globisch, R.J.B. Dietz, R.B. Kohlhaas, T. Göbel, M. Schell, D. Alcer, M. Semtsiv, and W.T. Masselink, J. Appl. Phys. **121**, 053102 (2017).
[15] J.B.D. Soole and H. Schumacher, IEEE J. Quantum Electron. **27**, 737 (1991).
[16] W.A. Wohlmuth, P. Fay, K. Vaccaro, E.A. Martin, and I. Adesida, IEEE Photonics Technol. Lett. **9**, 654 (1997).
[17] J.B.D. Soole and H. Schumacher, IEEE Trans. Electron Devices **37**, 2285 (1990).
[18] Jau-Wen Chen, Dae-Kaen Kim, and M.B. Das, IEEE Trans. Electron Devices **43**, 1838 (1996).
[19] J.H. Kim, H.T. Griem, R.A. Friedman, E.Y. Chan, and S. Ray, IEEE Photonics Technol. Lett. **4**, 1241 (1992).
[20] E. Dröge, E.H. Böttcher, D. Bimberg, O. Reimann, and R. Steingrüber, Electron. Lett. **34**, 1421 (1998).
[21] F.R. Bacher, J.S. Blakemore, J.T. Ebner, and J.R. Arthur, Phys. Rev. B **37**, 2551 (1988).
[22] M. Billet, P. Latzel, F. Pavanello, G. Ducournau, J.-F. Lampin, and E. Peytavit, APL Photonics **1**, 076102 (2016).
[23] T.W. Ebbesen, H.J. Lezec, H.F. Ghaemi, T. Thio, and P.A. Wolff, Nature **391**, 667 (1998).
[24] M. Billet, Y. Desmet, F. Bavedila, S. Barbieri, W. Hänsel, R. Holzwarth, G. Ducournau, J.-F. Lampin, and E. Peytavit, Electron. Lett. **53**, 1596 (2017).
[25] J.B. Kim, M.J. Kim, S.J. Kim, W.Y. Hwang, D.L. Miller, M.B. Das, J.M.M. Rios, and L.M. Lunardi, Opt. Quantum Electron. **29**, 953 (1997).
[26] M.G. Moharam, D. a. Pommet, E.B. Grann, and T.K. Gaylord, J. Opt. Soc. Am. A **12**, 1077 (1995).
[27] M. Billet and E. Peytavit, Opt. - Int. J. Light Electron Opt. **154**, 828 (2018).
[28] O. Svelto, in *Princ. Lasers* (Springer US, Boston, MA, 2010), pp. 131–161.
[29] E. Peytavit, M. Billet, Y. Desmet, G. Ducournau, D. Yarekha, and J.-F. Lampin, J. Appl. Phys. **118**, 183102 (2015).

FIG. 1

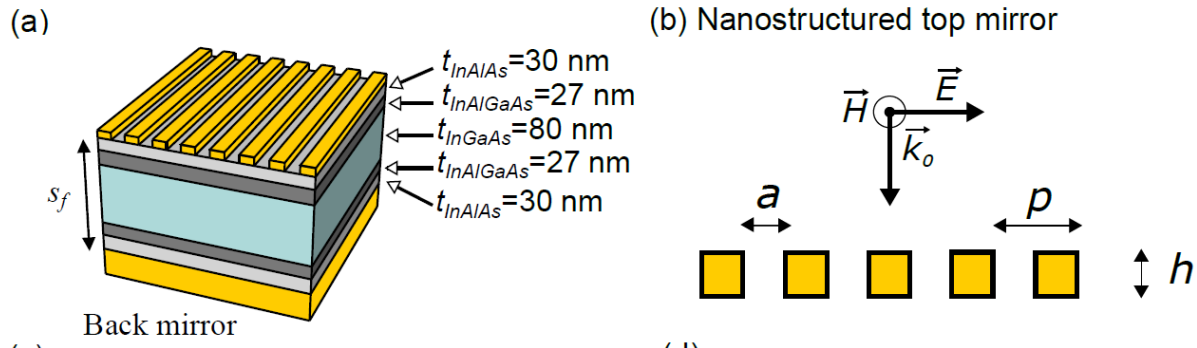

(c)

Material	Thickness
$In_{0.52}Al_{0.48}As$	30 nm
$In_{0.52}Al_{0.48}As/In_{0.53}Ga_{0.47}As$	27 nm
$In_{0.53}Ga_{0.47}As$	80 nm
$In_{0.52}Al_{0.48}As/In_{0.53}Ga_{0.47}As$	27 nm
$In_{0.52}Al_{0.48}As$	30 nm

(d)

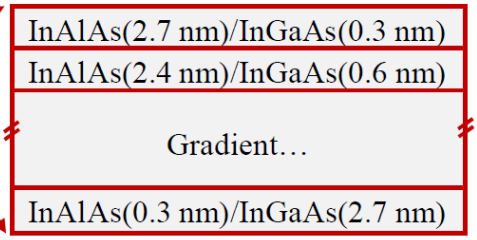

FIG. 1. Description of the RCE resonant cavity enhanced InAlAs/InGaAs-MSM (a) Schematic of the cavity (b) Nanostructured top mirror/electrode schematic (c) Semiconductor structure of the photodetector (d) Composition of the InAlAs/InGaAs graded layers.

FIG. 2

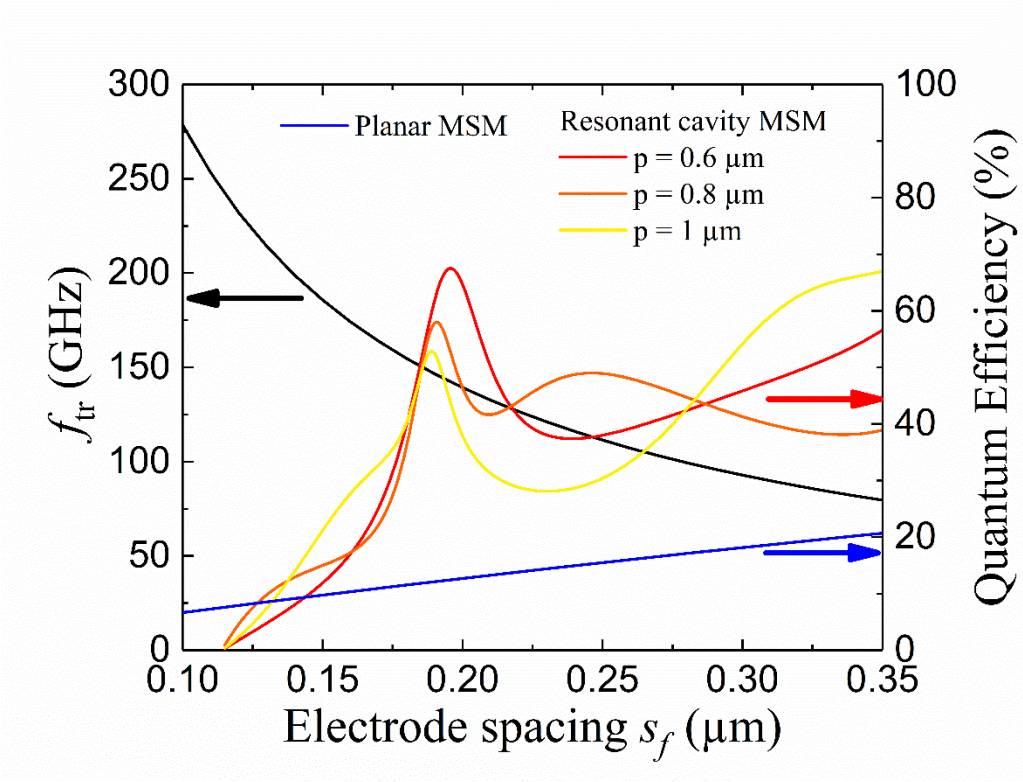

FIG. 2. Numerical calculation of quantum efficiencies for planar and resonant cavity InAlAs/InGaAs-MSMs with period p=0.6, 0.8 and 1 µm (a=0.3p and h=0.3 µm). Theoretical calculation of the transit time related cut-off frequency based on the free-carriers dynamic for planar and RCE InAlAs/InGaAs-MSMs.

FIG. 3

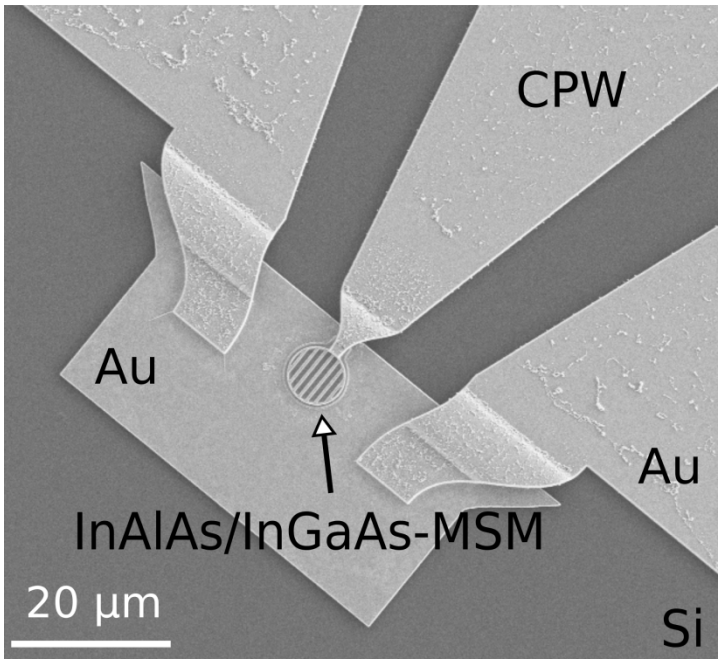

FIG. 3. SEM picture of a MSM photodetector integrated to a CPW waveguide.

FIG. 4

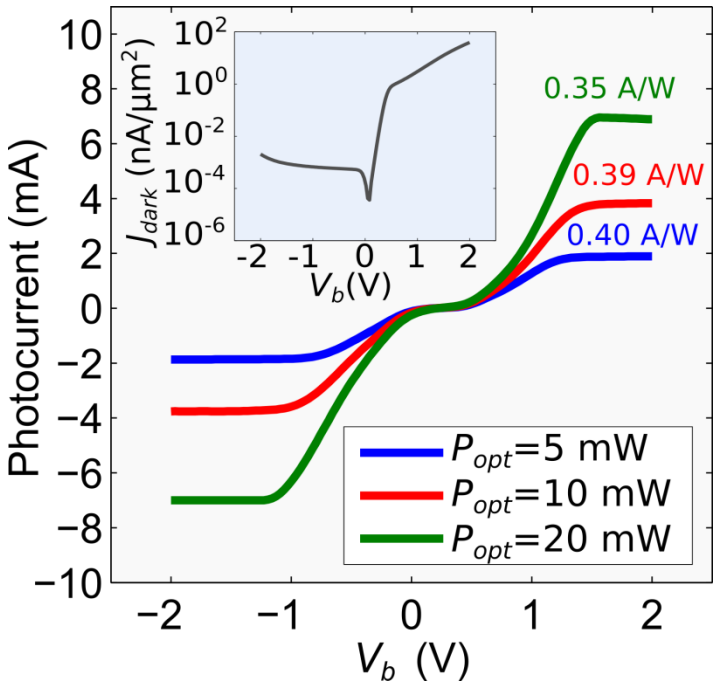

FIG. 4. Photocurrent as a function of bias voltage for different optical powers. Parameters of the nanostructured gold grating: p = 1 µm a = 300 nm h=300 nm. Inset: dark current density extracted from dark current measurement as a function of the bias voltage.

FIG. 5

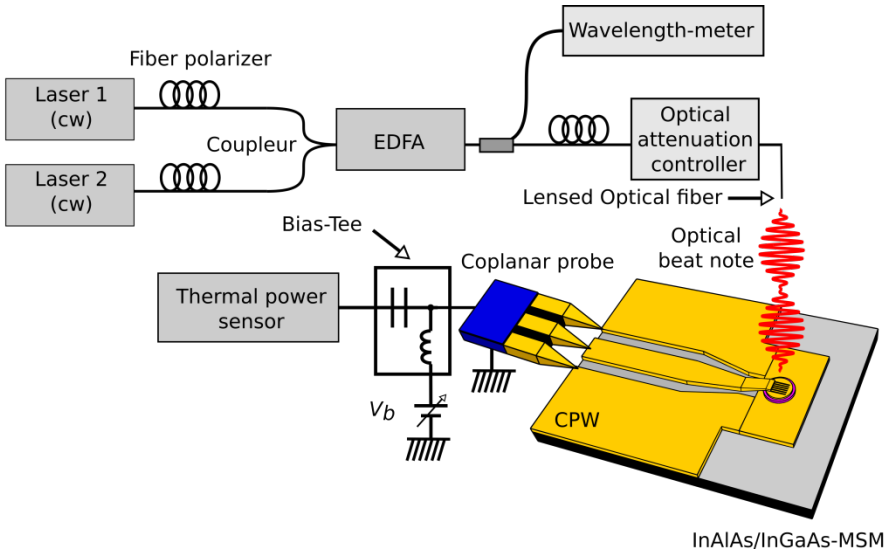

FIG. 5. Experimental set-up of the photomixing experiment.

FIG. 6

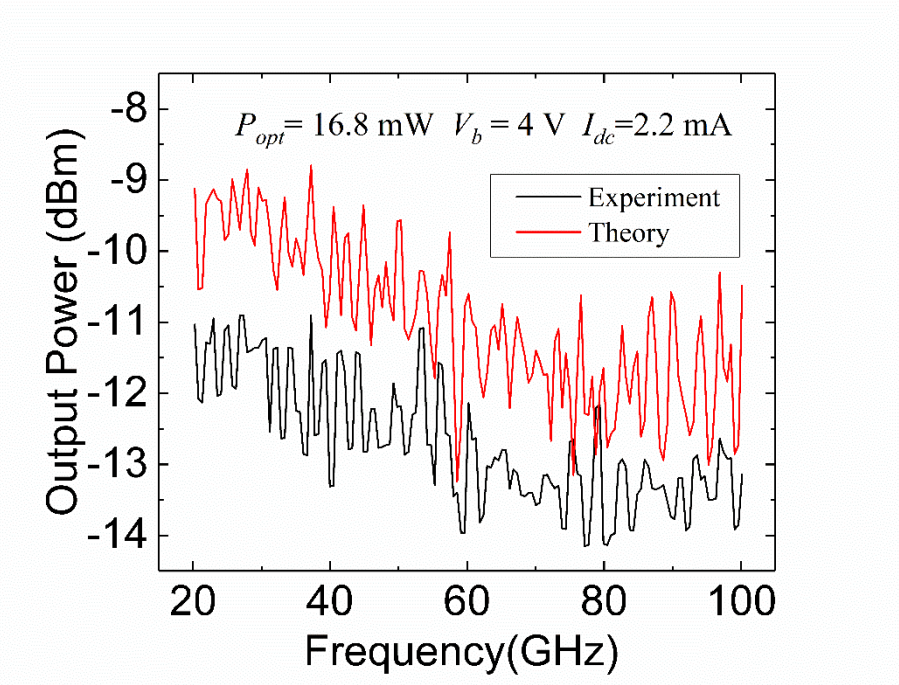

FIG. 6. Output sub-THz power as a function of the beatnote frequency. The nanoelectrode parameters are p = 0.6 μm, a = 180 nm and h = 0.3 μm.